# 13

# Tissue Fate Prediction from Regional Imaging Features in Acute Ischemic Stroke

Fabien Scalzo, Xiao Hu and David Liebeskind
*University of California, Los Angeles (UCLA)*
*USA*

## 1. Introduction

Stroke is a leading cause of death and a major cause of long term disabilities worldwide. According to the World Health Organization (WHO), a total of 15 million people suffer from a stroke each year comprising 5 million with a fatal outcome and another 5 million with permanent disabilities. While prevention research identifies factors and specific drugs that may lower the risk of a future stroke, the treatment of ischemic stroke patients aims at maximizing the recovery of brain tissue at risk. It is typically done by arterial recanalization of the vessel where the clot is located. Identification of salvageable brain tissue is essential during the clinical decision-making process. As a general rule for the decision to intervene, the expected benefits of the intervention should outweigh its potential risks and costs. To identify viable brain tissue, time is considered as a determining factor in the treatment of stroke patients. A perfect illustration of this timing issue is the thrombolytic therapy which uses specific drugs to break-up or dissolve the blood clot. As shown in a recent study (Hacke et al, 2008), thrombolysis applied with recombinant tissue plasminogen activator (rt-PA) is effective for acute ischemic stroke patients when administered intra-venously within a specific time window (3 hours, or 4 hours 30 min for patients meeting additional criteria). However, this time frame is arbitrary and might be too restrictive for some patients (Schaefer et al., 2007). For example, some patients could have benefited from this therapy but, instead, have been unnecessarily excluded. Beyond this ongoing debate about the length of the time window, there is a recognized need for accurate strategies to quantify the extent of viable tissue for victims of ischemic strokes and therefore to be able to identify the patients who could benefit from such a therapy.

Estimating the dynamic of infarct growth in ischemic stroke is extremely complex and its mechanisms are still poorly understood. Various factors such as quality of collateral perfusion, energy delivery, and age of the patient are known to have a significant impact on the outcome. However, their interactions over time is not clearly established and has not been quantified. The most commonly used techniques currently available to predict tissue outcome are based on imaging. It is widely accepted that the combination of diffusion (DWI) and perfusion-weighted (PWI) magnetic resonance imaging (MRI) provide useful information to identify the tissue at risk at an early stage. Several groups (Chen et al., 2008; Fisher & Ginsberg, 2004; Kidwell et al., 2004; Schlaug et al., 1999) have studied the mismatch between DWI and PWI to determine the penumbral tissue. However, DWI-PWI mismatch approaches have limitations: increased diffusion signals may be reversible (although a recent

study (Chemmanam et al., 2010) has concluded that it does not seem to be a common phenomenon), and the determination of the threshold of critical perfusion by PWI has been controversial (Heiss & Sobesky, 2005). DWI-PWI technique is based on the static thresholding of images and additional analysis is necessary to predict the final infarct size.

More recently, considerable attention has been given to the development of automatic, quantitative predictive models that can estimate the likely evolution of the endangered tissue. These approaches that have been proposed in the literature differ on the types of images, and the prediction techniques they employ. Initially, automatic prediction models have been trained on a voxel-by-voxel basis by integrating multimodal perfusion information from cases with known follow-up tissue fate. WU *et al* (Wu et al., 2001; 2007) proposed in one of their studies a framework based on a generalized linear model (GLM) and evaluated 14 ischemic stroke patients. Results showed that combining parameters computed from DWI and PWI offers higher specificity and sensitivity than models trained on DWI, or PWI alone. ROSE *et al* (Rose et al., 2001) used Gaussian models trained on multiple parameters (DWI, CBF, CBV, mean transit time (MTT)) to predict tissue outcome on 19 ischemic stroke patients. Other studies based on logistic regression (Yoo et al., 2010), on ISODATA clustering (Shen et al., 2005) applied to ADC and CBF have also led to similar conclusions; the combination of various parameters improves the prediction accuracy. In addition to the DWI-PWI mismatch, several studies (Olivot, Mlynash, Zaharchuk, Straka, Bammer, Schwartz, Lansberg, Moseley & Albers, 2009; Olivot, Mlynash, Thijs, Purushotham, Kemp, Lansberg, Wechsler, Gold, Bammer, Marks & Albers, 2009) have demonstrated that time-to-maximum (Tmax) of the residue function is a reliable parameter to detect penumbra in acute stroke because it implicitly captures a complex combination of delay and dispersion. It has been shown to predict actual CBF more accurately than mean transit time (MTT) (Olivot, Mlynash, Zaharchuk, Straka, Bammer, Schwartz, Lansberg, Moseley & Albers, 2009).

The regional information contained in the surrounding voxels of the location to be predicted has been shown in recent works to improve the accuracy of the predictive model in comparison with a single-voxel-based method. Although some regional information may implicitly be included by single-voxel-based methods via the convolution of the image with a smoothing filter, it is usually not taken into account by the models. Promising approaches have attempted to take into account the regional distribution explicitly by exploiting spatial correlation between voxels (Nguyen et al., 2008), using a prior map of spatial frequency-of-infarct (Shen & Duong, 2008), and Neural Networks (Huang et al., 2010). All these studies have demonstrated signs of improvement in comparison with single-voxel-based approaches.

Drawing from these findings, this chapter introduces a predictive model of tissue fate that captures the relationship between spatial patterns observed in perfusion images after onset and tissue outcome. This work presents a comparative analysis of the predictive power of different flow parameters extracted from Perfusion Weighted Images (PWI) during the acute phase of the stroke. Specifically, Cerebral Blood Volume (CBV), Cerebral Blood Flow (CBF), Mean Transit Time (MTT), Tmax, Time-To-Peak (TTP), and Peak are extracted and evaluated in this study. The predictive model is formalized as a nonlinear regression problem. It combines the tissue information available at onset in terms of Fluid Attenuated Inversion Recovery (FLAIR) images with parameters extracted from PWI to predict the tissue outcome four days after intervention. FLAIR images are used in this study to identify lesions from previous strokes and, to a lesser extent, early lesions in the acute phase. They are also used to assess the survival outcome of the brain tissue four days after intervention. While FLAIR

is the gold standard in neurology to depict irreversible lesions, PWI parameters represent flow-related features that may be useful for the prediction of tissue outcome.
The novelty of the proposed work is to study the impact of a regional model on each of these perfusion maps (CBV, CBF, MTT, Tmax, Peak, TTP). The regional distribution among neighboring voxels is represented by *cuboids* (*i.e.* rectangular volumes) (Fig 1(a)). By varying the size of these cuboids, we expect to determine what is the optimal size for each map that leads to the most accurate tissue fate prediction. Such an approach can be seen as a 3D generalization of subwindows-based stochastic methods (Maree et al., 2005) that have been successfully used on a wide variety of image classification problems.
During learning, the cuboids are sampled at similar locations in FLAIR and one of the perfusion images, and each pair of cuboids is combined into a single vector and used as input to the predictive model. The output is the tissue fate, in terms of FLAIR voxel intensity, measured 4-days after an arterial recanalization intervention. A Kernel Spectral Regression (SR-KDA) (Cai et al., 2007) model is used to represent the relation that exists between PWI parameters combined with FLAIR images at onset and the tissue fate.

## 2. Image-based prediction of tissue outcome

### 2.1 Patients, and MRI data acquisition

MRI data was collected from patients identified with symptoms of ischemic stroke and admitted at the University of California-Los Angeles Medical Center. The use of these data was approved by the local institutional review board (IRB). Inclusion criteria for this study included: (1) presenting symptoms suggestive of acute stroke, (2) last known well time within six hours, (3) MRI (including PWI) of the brain performed before recanalization therapy and approximately four days later, (4) final diagnosis of ischemic stroke. A total of 25 patients (mean age, $56 \pm 21$ years; age range, 27 to 89; 15 women; average NIHSS of $14 \pm 6.3$) satisfied the above criteria and underwent MRI using a 1.5 Tesla echo planar MR imaging scanner (Siemens Medical Systems). The PWI scanning was performed with a timed contrast-bolus passage technique (0.1 mg/kg contrast administered intravenously at a rate of 5 cm3/s) and with the following parameters on average: repetition time (TR), 2000 ms; echo time (TE), 60 ms. The FLAIR sequence was acquired with the following parameters: repetition time (TR), 7000 ms; echo time (TE), 105 ms; inversion time (TI), 2000 ms. All the images were resized using bilinear interpolation to match a resolution of $1 \times 1 \times 5$ mm per voxel.
The median time from symptom onset to baseline MRI was 4h38 (IQR 1h43, 5h39), and to followup MRI was 4 days 13h30 (IQR 3 days 15h08, 4 days 22h17). Median time from onset to intervention was 6h20. The degree of success of the intervention in terms of recanalization and reperfusion, as well as the quality of collaterals have a significant impact on the tissue fate. These factors are not taken into account in our predictive model because it relies only on onset images.

### 2.2 Prediction framework

The prediction framework proposed in this chapter relies on a regression model that is learned in a supervised fashion from a set of training images with known outcome. Once the model has been trained, it can be used to predict the tissue fate, in terms of followup FLAIR intensity, on new cases. The following subsections describe a series of preprocessing steps (Figure 1(b)) prior to the predictive modeling.

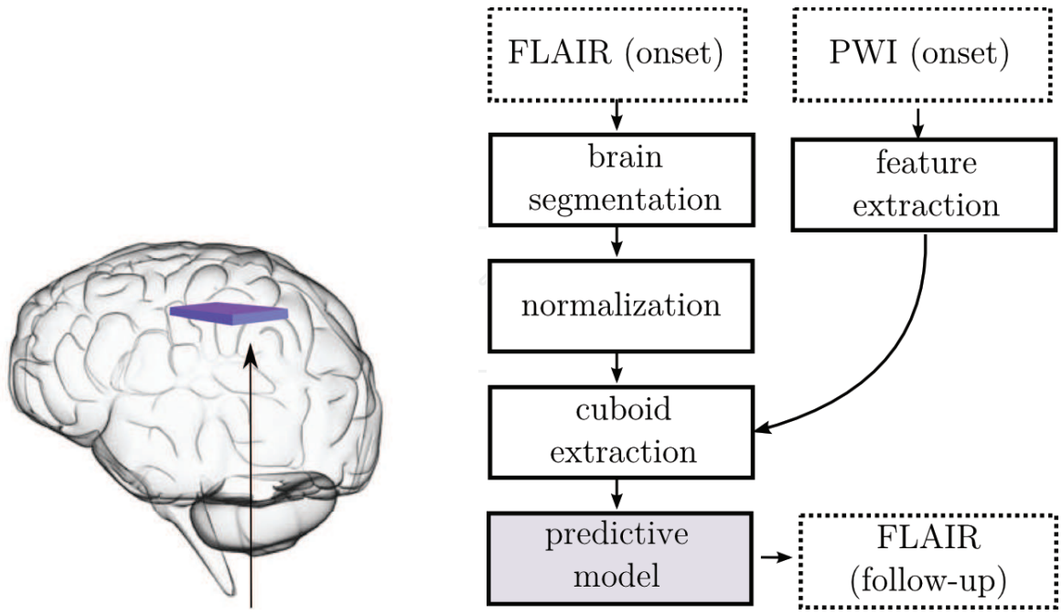


(a) Cuboid (b) Prediction Framework

Fig. 1. (a) Illustration of a cuboid extracted from the brain volume. (b) During prediction, the skull is first stripped from the FLAIR image and the result is normalized. A parameter map is extracted from PWI images and registered to FLAIR images. Cuboids are sampled at the same locations from both images and used as input to the regression model to predict the tissue outcome.

#### 2.2.1 Automatic brain volume segmentation

Before learning, the framework requires FLAIR images acquired immediately after onset and at followup to be co-registered. The skull and non-brain tissue could interfere with the registration process and therefore have been stripped.

To perform this brain extraction step, we use the FSL Brain Extraction Tool (BET) (Smith., 2002) that is integrated into a pipeline software developed by the Laboratory of Neuro Imaging (LONI) at UCLA (`http://www.loni.ucla.edu/`). BET estimates an intensity threshold to discriminate between brain/non-brain voxels. Then, it determines the center of gravity of the head, defines a sphere based on the center of gravity of the volume, and finally deforms it toward the brain surface.

#### 2.2.2 FLAIR image normalization

Because FLAIR images were acquired with different settings and originated from different patients, their intensity value was not directly comparable. To allow for inter-patient comparisons, FLAIR images were normalized with respect to the average intensities within the contralateral white matter. The normal-appearing white matter was delineated manually by an experienced researcher for both onset and follow-up brain volumes.

#### 2.2.3 Perfusion imaging features

Imaging features are extracted from PWI images with a software developed at UCLA, the Stroke Cerebral Analysis (SCAN) package. The tissue contrast agent concentration $C(t)$ is expressed as a convolution of the arterial input function (AIF) identified from the contralateral

middle cerebral artery (MCA) and the residue function $R(t)$ (Calamante et al., 2010)

$$C(t) = CBF \times (AIF(t) \otimes R(t)), \tag{1}$$

where $CBF$ is the cerebral blood flow. The residue function is obtained by deconvolution, and the time to its maximum value is used to specify Tmax. Therefore, Tmax is the arrival delay between the AIF and C(t).
After applying a gamma variate fit on a pixel-by-pixel basis, cerebral blood volume (CBV) is estimated in each voxel by computing the area under the fitted gadolinium concentration time curve, measured in the corresponding image pixel at every time point after bolus arrival:

$$CBV = \sum_{t=0}^{N_c} C(t). \tag{2}$$

The mean transit time (MTT) is computed as the normalized first moment of the fitted curve, up to the peak of the curve. The time to peak contrast concentration (TTP) is another perfusion-related parameter that corresponds to the time it takes for signal intensity to reach its minimum in each pixel. The value of this minimum is used to define another feature called Peak.
Finally, CBV and MTT are used to calculate the cerebral blood flow (CBF) through the tissue voxel, according to the central volume theorem:

$$CBF = \frac{CBV}{MTT}. \tag{3}$$

#### 2.2.4 Image registration

Registration of FLAIR and PWI images is necessary because the outcome of an extracted cuboid, measured as a voxel value in the followup image, has to correspond to the same anatomical location in the different volumes. Co-registration was performed for each patient independently. Because the intensity of FLAIR images may present large variations between onset and followup due to changes in the tissue perfusion caused by the stroke, several attempts to use automatic image registration methods failed to accurately align the volumes. Instead, our framework utilized five landmark points placed manually at specific anatomical locations (center, plus four main cardinal directions) on the slice of the brain that had the largest ventricular area. An affine projection was applied to project the followup FLAIR and acute Tmax on the original FLAIR volume.

#### 2.2.5 Ground truth

During evaluation, we pose the prediction task as a two-class classification problem, where the voxel of the groundtruth is set to 1 if it is infarcted and 0 if it is not. The groundtruth is obtained by manual outline of infarcts on FLAIR images by an expert in neurology from UCLA who was asked to precisely delineate infarcts, comparing the infarcted hemisphere with the contralateral hemisphere. Outlining was performed with the help of the commercially available medical imaging software 3D DOCTOR developed by ABLE SOFTWARE CORP (`http://www.ablesw.com/`). No manual outlining is made on the predicted images.

### 2.2.6 Cuboid sampling

For training, we exploit a set of FLAIR images $F$ at onset, their corresponding co-registered PWI feature map $M$, and followup FLAIR images $F'$.

The dataset $\{X, Y\}$ used to train and to evaluate the predictive model is created by extracting cuboids of fixed size $w \times l \times d$ among onset images with their corresponding outcome. Each cuboid $c \in \mathbb{R}^s$ is described by its raw voxel values, yielding an input vector of $s = w \times l \times d$ numerical attributes. Our method extracts a large number of cuboids at random positions from training images. In practice, given a sampled location $\{i, j, k\}$, we extract a cuboid $c_F$ in the acute FLAIR image at $F(i, j, k)$ and a corresponding cuboid $c_M$ in the perfusion map at $M(i, j, k)$. To improve the generalization power of the predictive model, the cuboids $c_M, c_F$ are normalized with respect to the direction $\theta$ of the image gradient in the XY plane using an image rotation, performed with bilinear interpolation. Normalized patches $c_{M'}, c_{F'}$ thus become invariant to orientation changes in the XY plane. Orientation normalization is particularly useful when considering the case where cuboids are located at the same distance from a circular infarction but at different directions. If no rotational normalization is performed, all the cuboids have a different appearance and the model has to be trained for all the directions around the infarct and requires more training examples.

$$c_{M'} = \text{imrotate}(c_M, -\theta_M) \qquad \theta_M = \tan^{-1} \frac{L^{\sigma}_{y,M}(x, y, z)}{L^{\sigma}_{x,M}(x, y, z)} \tag{4}$$

$$c_{F'} = \text{imrotate}(c_F, -\theta_F) \qquad \theta_F = \tan^{-1} \frac{L^{\sigma}_{y,F}(x, y, z)}{L^{\sigma}_{x,F}(x, y, z)} \tag{5}$$

where $L^{\sigma}_{x,F}$, $L^{\sigma}_{x,F}$, $L^{\sigma}_{x,M}$, $L^{\sigma}_{y,M}$ are the Gaussian derivatives in X and Y directions, computed from the acute FLAIR image $F$ and perfusion map $M$,

$$L^{\sigma}_{x,M} = \frac{\partial}{\partial x} \mathcal{G}_{\sigma} \otimes M \qquad L^{\sigma}_{y,M} = \frac{\partial}{\partial y} \mathcal{G}_{\sigma} \otimes M \tag{6}$$

$$L^{\sigma}_{x,F} = \frac{\partial}{\partial x} \mathcal{G}_{\sigma} \otimes F \qquad L^{\sigma}_{y,F} = \frac{\partial}{\partial y} \mathcal{G}_{\sigma} \otimes F \tag{7}$$

where $\mathcal{G}_{\sigma}$ is a 2D isotropic Gaussian filter with standard deviation $\sigma = 3$ in our experiments. The two cuboids are merged into a single, multi-modal cuboid $x = \{c_{F'}, c_{M'}\}$ that corresponds to the concatenation of the cuboids extracted at the same location in the different volumes. Each multi-modal cuboid $x$ is then labeled with the intensity $y$ of the central voxel in the corresponding follow-up FLAIR image $y = F'(i, j, k)$. The dataset consists of the set of multi-modal cuboids $x \in X$ and their corresponding outputs $y \in Y$ that represent the followup FLAIR intensities.

### 2.3 Regression-based predictive model

Our predictive model takes the form a regression model $y = f(x)$ that maps the tissue outcome $y \in Y$, described in terms of the voxel intensity in the followup FLAIR image, as a function of the multi-modal cuboid $x \in X$ extracted at the same location. Defining outputs $y$ in a continuous space, in contrast with a binary one, allow us to easily change the sensitivity and specificity of the framework, by varying the threshold on the predictions. A greyscale (or color) output image is also more adapted than a binary image to visualize complex patterns.

In the context of pattern recognition, the literature of regression analysis has been particularly proficient in the last couple of years with the emergence of robust, nonlinear methods. In

this study, the comparative analysis will be based on a Kernel Spectral Regression (SR-KDA) analysis (Cai et al., 2007) that we successfully used in our preliminary study (Scalzo et al., 2010), and other regression-based pattern recognition applications Scalzo et al. (2009; 2010).

#### 2.3.1 Kernel spectral regression

Kernel Spectral Regression (SR-KDA) (Cai et al., 2007) is a recently proposed method to solve Kernel Discriminant Analysis (KDA) problems efficiently. Specifically, it poses the discriminant analysis as a regularized regression problem that exploits a graph representation. SR-KDA utilizes a kernel projection of the data (also called "kernel trick" in the literature). Input data samples $X$ are projected onto a high-dimensional space via a Gaussian kernel $K$,

$$K(i,j) = \exp -\|x_i - x_j\|^2 / 2\sigma^2 \tag{8}$$

where $\sigma$ is the user-specified standard deviation of the kernel.
In addition, from the set of $n$ input data samples $X$, a $n \times n$ symmetric affinity matrix $W$ is generated with $W_{ij}$ having a positive constant value if $x_i, x_j \in X$ are from the same class (i.e. $y_i \in Y$ is equal to $y_j \in Y$), and zero otherwise. From matrix $K$ and $W$, SR-KDA uses the Gram-Schmidt method to obtain eigenvectors $\phi$,

$$W\phi = \lambda\phi \tag{9}$$

and estimates the mapping $\alpha$ efficiently using a Cholesky decomposition,

$$\alpha^{\mathrm{T}}(K + \delta I) = \phi \tag{10}$$

where $I$ is the identity matrix, $\delta > 0$ the regularization parameter, and $\phi$ are the eigenvectors of $W$. When a new multi-modal cuboid, $x_{\mathrm{new}}$, is extracted from the image of a new patient, the FLAIR intensity at followup, $\hat{y}_{\mathrm{new}}$, is computed using

$$k(i) = \exp -\|x_i - x_{\mathrm{new}}\|^2 / 2\sigma^2, i = 1 \ldots n \tag{11}$$

$$\hat{y}_{\mathrm{new}} = \hat{\alpha}^{\mathrm{T}}(k + \delta I) \tag{12}$$

where $k$ is the vector resulting from the kernel projection of $x_{\mathrm{new}}$ into the kernel space using training data $X$.

### 2.4 Experimental setup

This section describes how the predictive power in terms of tissue fate of the different perfusion images will be evaluated on our dataset of ischemic stroke patients. The proposed experiments are designed to answer the following questions: *Do the neighboring voxels significantly improve the prediction of the tissue outcome at a specific voxel in the different maps? If so, what is the optimal size of this neighborhood in ischemic strokes? Does it differ depending on the type of image?* Specifically, these questions will be addressed by evaluating the tissue fate prediction accuracy of the Kernel Spectral Regression (SR-KDA) (Section 2.3.1) method on our dataset (Section 2.1). The problem is posed as a classification task where the output $Y$ (*i.e.* followup FLAIR image) was manually binarized to create the ground truth (Section 2.2.5).
A specific model will be trained for each of the six types of perfusion parameter; CBV, CBF, MTT, Tmax, TTP, Peak. The training of a specific regression model is made from a set of training samples that, in the ideal case, should be uniformly distributed throughout the data space. However, this is not the case for most of the stroke patients where the brain volume

contains a larger number of noninfarcted voxels. A recent study (Jonsdottir et al., 2009) has shown that an unequal number of infarcted and noninfarcted voxels can negatively impact the overall performance of the system. Following the methods of the study, we perform a random sampling on the input cuboids so that an equal number of infarcted and noninfarcted cuboids are present in the training set. The number of training samples for each slice was set to a maximum of 85 cuboids of class 0 and 85 cuboids of class 1. In theory, this could create a large dataset of $170 \times nbSlice \times nbCases$ training samples. In practice, however, we reduce the size of the dataset during the extraction process such that the number of extracted cuboids for a slice is equal to the minimum number of occurrence of either class (0 or 1). For example, if only 10 voxels are infarcted (class 1) on the followup of one slice, only 10 cuboids will be extracted for class 1 as well as 10 other cuboids for class 0. This procedure has the advantage of speeding up the cuboid extraction process and generates less than $10,000$ training samples equally distributed between the two classes.

#### 2.4.1 Cuboid size

For each PWI parameter map, we evaluate the accuracy of the SR-KDA regression method to predict tissue fate for different sizes of cuboids. A predictive model is evaluated for each cuboid size using a leave-one-patient-out crossvalidation so that the data from the patient evaluated is excluded from the training set at each iteration. In this experiment, cuboids are symmetric; $w$, $l$ have the same length (Section 2.2.6). The tested sizes [1] spanned from $1 \times 1$ to $23 \times 23$. During the leave-one-out crossvalidation, the Area Under the Curve (AUC) is computed from the ROC curve for each patient. The average AUC and standard deviation across patients are calculated and constitute our measure of performance. The parameters of SR-KDA $\sigma, \delta$ were optimized at each iteration of the leave-one-out procedure by running another leave-one-out cross-validation on the data excluding the patient to be tested.

#### 2.4.2 Global ROC curves

Global ROC curves are also generated for each PWI parameter map. For fair comparison, the cuboid size of each image was the one that led to the best accuracy in the experiment presented in the previous paragraph and reported in Figure 2. To generate the global ROC curve, predictions $\hat{Y}_i$ are first computed for each specific patient $i$ during the crossvalidation. Then, all the prediction vectors $\{\hat{Y}_1, \hat{Y}_2, \ldots, \hat{Y}_n\}$ are concatenated into a single vector $\hat{Y}_{total}$, and the global ROC curve is computed from the data of all patients $\hat{Y}_{total}$.

#### 2.4.3 McNemar's significance test

Although differences in average AUCs can be used to rank the predictive power of the different PWI parameter maps and to observe the improvements of the regional model versus a single-voxel-based approach, differences are not necessarily statistically significant. We propose to use a McNemar's test (Siegel & Castellan, 1988) to verify if the difference between between regional and single-voxel-based models are statistically significant for each PWI map. McNemar's test, which is based on a Fisher-test with one degree of freedom, is a useful tool in determining if two methods have comparable error rates. Given the null hypothesis that the two methods A and B have the same error rate, and the following contingence table (Table 1),

[1] The low sagittal resolution ($\geq$ 7 mm per voxel) of PWI images did not allow us to test the $z$-size of the cuboid which was set to 1 slice.

McNemar's test can be written as a Fisher-test,

$$\chi^2 = \frac{(|b-c|-1)^2}{b+c}. \tag{13}$$

| | Correct (B) | Error (B) | Total |
|---|---|---|---|
| Correct (A) | a | b | a+b |
| Error (A) | c | d | c+d |
| | a+c | b+d | n |

Table 1. Classification contingence table between two methods (A, B).

McNemar's test is applied to investigate if the main hypothesis of this paper is supported by a statistical significance test. We verify that the improvement in performance obtained by the regional cuboids versus a single voxel is significant. To do so, the McNemar's test is performed between the models obtained using SR-KDA with their optimal cuboid size and with a single voxel $1 \times 1$. We perform the experiment for each PWI parameter map with the following optimal cuboids size (identified in the previous experiment): Tmax, $15 \times 15$; MTT, $15 \times 15$; CBV, $9 \times 9$; CBF, $11 \times 11$; TTP, $13 \times 13$; Peak, $11 \times 11$.

## 3. Results

### 3.1 Cuboid size

AUC after a leave-one-patient-out crossvalidation for an increased cuboid size is reported in Figure 2 for each PWI parameter map. The AUC can be interpreted as the probability of correct classification for a randomly selected pair of positive and negative samples. Usually, any AUC result above .9 is considered as excellent.

Baseline average accuracy for Tmax parameter reaches $0.83 \pm 0.01$ with cuboid size $1 \times 1$ and increases to $0.90 \pm 0.05$ at a size of $15 \times 15$. MTT parameter reaches $0.76 \pm 0.02$ and increases to $0.87 \pm 0.06$ at a size of $15 \times 15$. CBV parameter reaches $0.67 \pm 0.03$ and increases to $0.74 \pm 0.10$ at a size of $9 \times 9$. CBF parameter reaches $0.71 \pm 0.02$ and increases to $0.81 \pm 0.08$ at a size of $11 \times 11$. TTP parameter reaches $0.84 \pm 0.02$ and increases to $0.91 \pm 0.04$ at a size of $13 \times 13$. Peak parameter reaches $0.74 \pm 0.02$ and increases to $0.82 \pm 0.08$ at a size of $11 \times 11$.

These results suggest that Tmax and TTP parameters are the most accurate single maps to predict the tissue outcome. Interestingly, the optimal size of the cuboids vary across the different modalities, however all of them outperform their respective single-voxel-based model. These results demonstrate that a regional approach, which takes into account neighboring voxels may improve the prediction accuracy regardless of the modality used.

Global ROC curves that illustrate the results in terms of true positive and false positive rates are depicted in Figure 3. The ROC are produced for each parameter map, comparing the results between a baseline cuboid size of $1 \times 1$ and the optimal size.

The similarity between the prediction and the actual outcome of the brain tissue for each parameter can be visualized in Figure 4 on arbitrary slices. The columns respectively correspond (from left to right, top to bottom) to follow-up FLAIR, prediction from Tmax, TTP, MTT, the manually outlined ground truth of followup FLAIR, and prediction from CBV, CBF, and Peak. The prediction are produced from the SR-KDA model trained using a leave-one-out crossvalidation with optimal cuboid size for each modality.

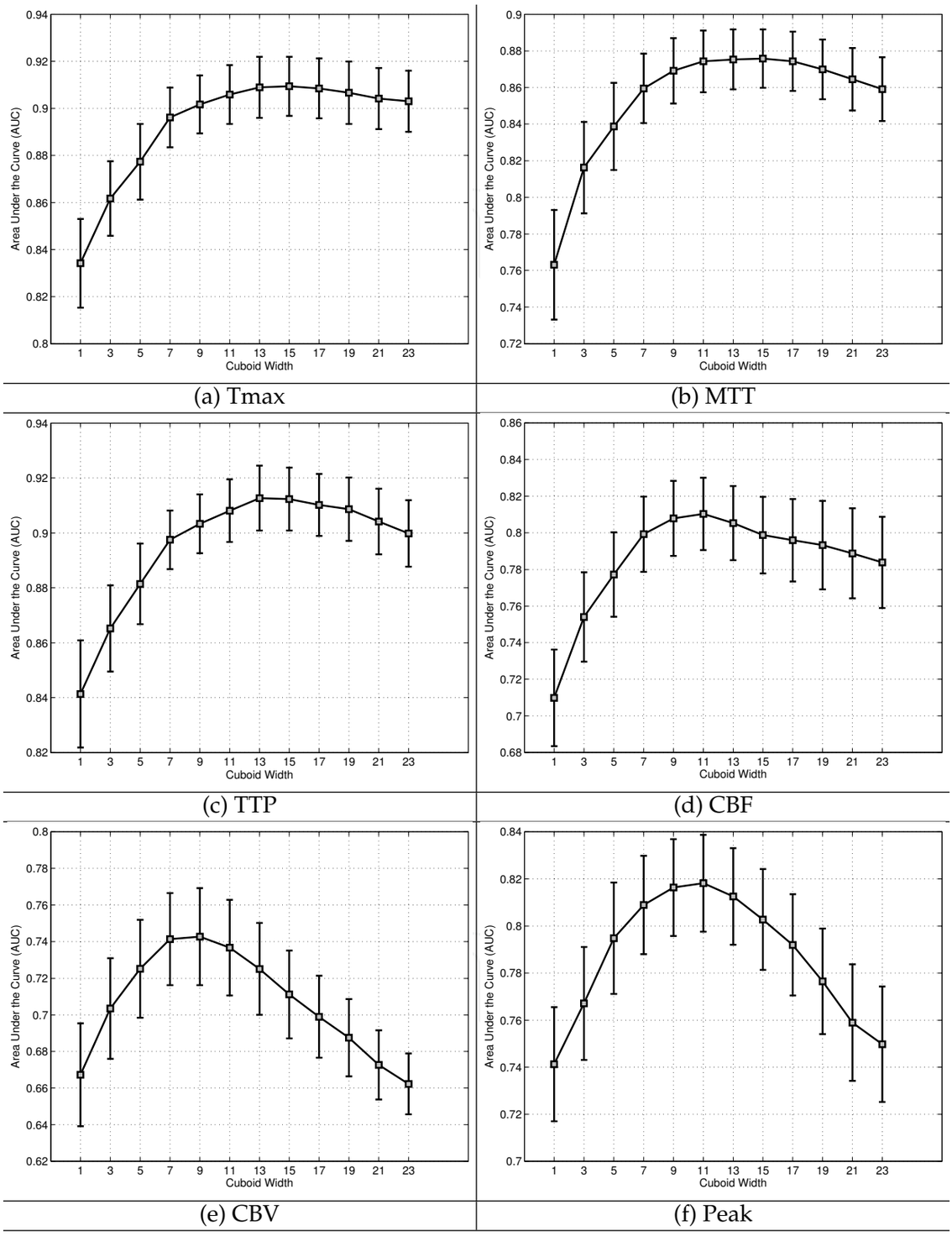


Fig. 2. Effect of the cuboid size on the average Area Under the Curve (AUC) for SR-KDA regression models using a leave-one-out crossvalidation strategy.

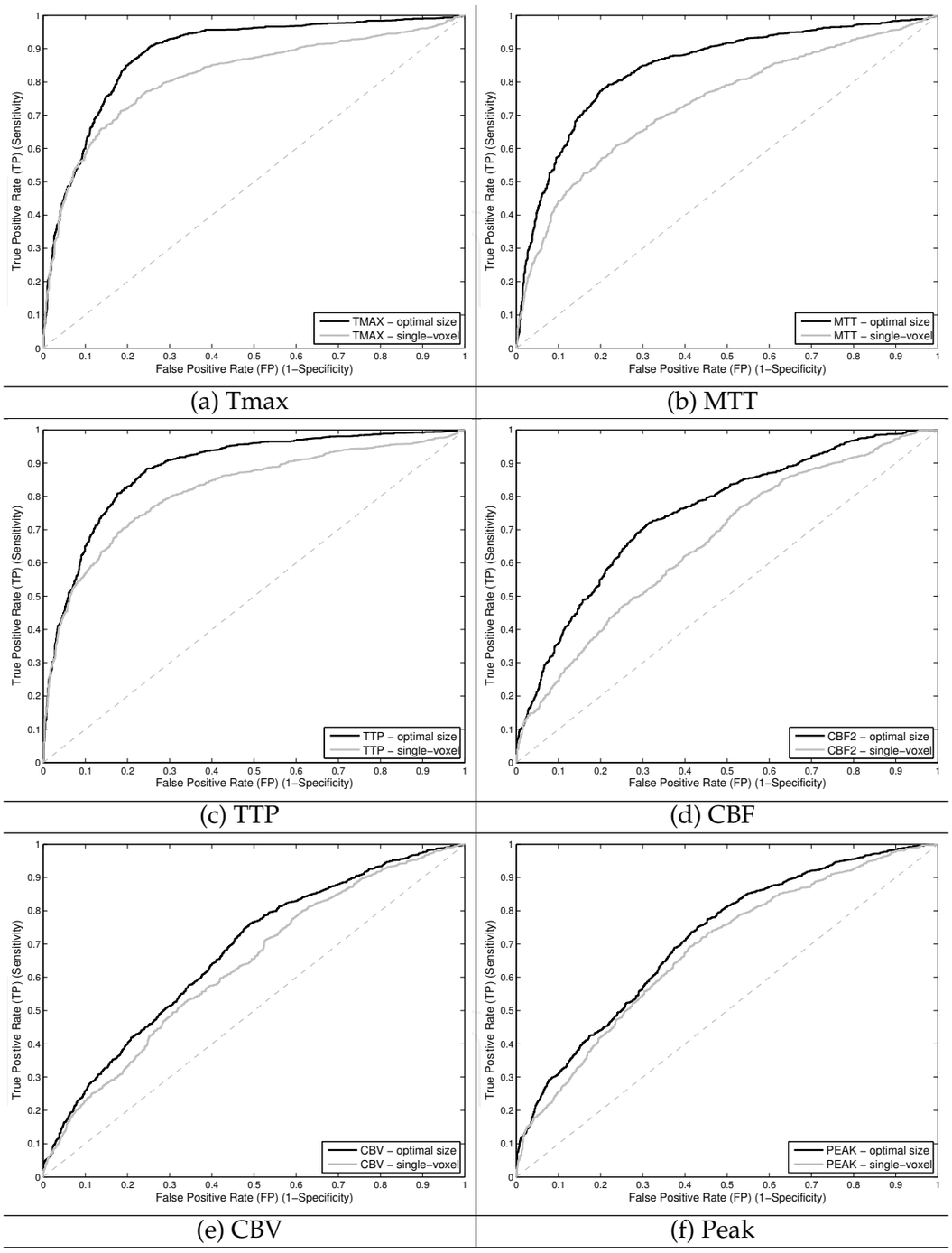


(a) Tmax (b) MTT

(c) TTP (d) CBF

(e) CBV (f) Peak

Fig. 3. For each parameter, ROC curves (dark line) are generated using the cuboid size that led to the best average AUC for each method as reported in Fig 2, and compared to single-voxel-based models (gray line). The difference between the dark and gray lines is proportional to the improvement obtained by a regional model versus single-voxel-based model.

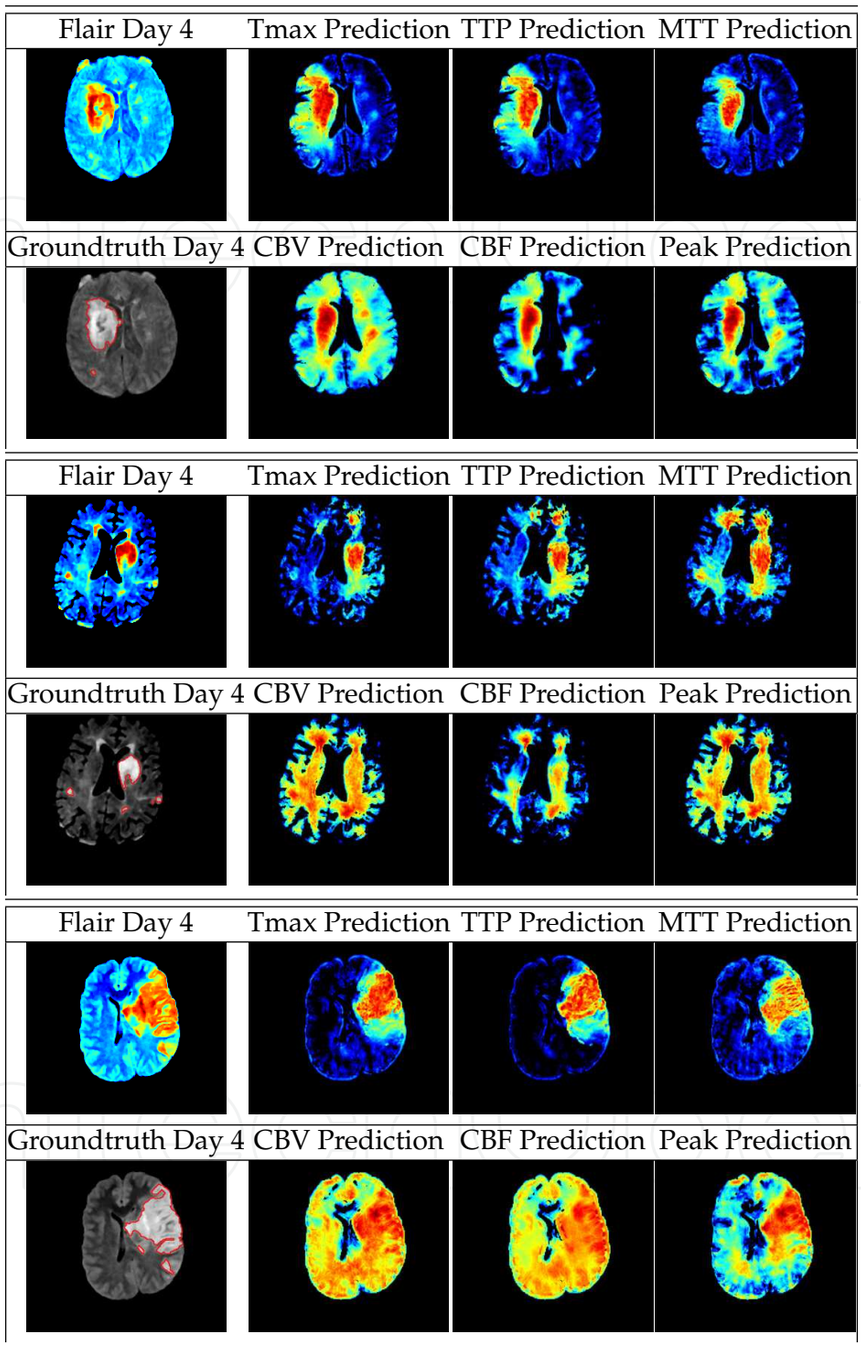


Fig. 4. Prediction results for three patients. FLAIR at followup, and predictions from onset Tmax, TTP, MTT, perfusion map are illustrated on the first row. Predictions are compared to the ground truth manually outlined in followup FLAIR at day 4 on the second row, followed by CBV, CBF, and Peak predictions.

### 3.2 McNemar's test

Significance results of the McNemar's test are summarized in Table 2. With a 95% confidence interval and one degree of freedom, two models are considered significantly different if the value $\chi^2$ is above 3.8414. McNemar's values between a baseline model of size $1 \times 1$ versus an optimal regional model are $25.56, 116.8, 54.04, 5.81, 23.31 3.12$, for Tmax, MTT, TTP, CBF, CBV, Peak, respectively. Because they are way over 3.8414, regional models for Tmax, MTT, CBF, CBV (and CBF to some extent) can be considered to improve the prediction accuracy significantly. However, Peak was just below the threshold and therefore the impact of the regional model on this feature map cannot be considered significant on our dataset.

| Test | McNemar value |
|---|---|
| Tmax 15x15 vs Tmax 1x1 | 25.56 |
| MTT 15x15 vs MTT 1x1 | 116.8 |
| TTP 13x13 vs TTP 1x1 | 54.04 |
| CBF 11x11 vs CBF 1x1 | 5.81 |
| CBV 9x9 vs CBV 1x1 | 23.31 |
| Peak 11x11 vs Peak 1x1 | 3.12 |

Table 2. Results of McNemar's test to measure the significance of using single-voxel-based versus regional models using the optimal cuboid size for each PWI parameter map.

### 3.3 Computational performance

The predictive model was implemented in Matlab and executed on a Dell Optiplex 760 desktop computer equipped with an Intel Core2 Duo CPU cadenced at 3.33GHz. The training of the predictive model, excluding image normalization, volume registration, and ground truth selection took less than ten minutes for $10 \times 10$ cuboids, while the prediction on an entire volume took less than two minutes. Note that the speed depends on the size of the cuboids, larger cuboids require more memory and computational time.

## 4. Discussion

The prediction of brain tissue fate in ischemic stroke, and therefore the identification of salvageable tissue, is a challenging problem that holds useful information for the clinician during the decision making process. Ultimately, automatic tissue fate predictive models could help us understand the underlying mechanisms of infarct growth. These mechanisms are complex, as they depend on a wide variety of factors such as: quality of blood perfusion to the area, quality of colaterals, energy delivery, age and medical history of the patient, etc. Integrating all these elements within a unified predictive model is the long-term goal of our research.

In this chapter, we have proposed a comparative analysis about the predictive power of PWI parameter maps. A generic framework based on a nonlinear regression method was introduced to predict the likely outcome of brain tissue in ischemic stroke patients. Although the models were trained on a rather small dataset (25 patients), our experimental results have demonstrated that significant improvement can be obtained by a regional model in comparison with a single-voxel-based approach. Several feature maps achieve an average

AUC of over .8 using optimal cuboid sizes. These good performances may be explained by the three following reasons:

- Regional: The use of optimized cuboids significantly improves a single-voxel-based approach. A possible explanation of this improvement is that cuboids implicitly represent the regional distribution of intensity and correlation among voxels and are more robust to noise.
- Nonlinear: The predictive model is based on Kernel Spectral Regression (SR-KDA) that has demonstrated excellent performances in a wide variety of applications. For the current application, a possible explanation for this difference is that the relation between the cuboids extracted at onset from PWI parameters and the followup FLAIR intensity is not a linear one, and it is, therefore, better captured by a nonlinear model such as SR-KDA.
- Randomness: Because machine learning techniques are often limited in the number of training samples they can handle in a reasonable time, efficiently exploiting the millions of cuboids available in the training set is a complex task. To obtain a representative training set, we randomly sample cuboids across images so that a similar number of cuboids is sampled for each outcome (infarcted or not). This is similar in spirit to what has been shown in a previous study (Jonsdottir et al., 2009).

In principle, even after normalization, FLAIR images are not necessarily comparable between patients. However, in practice, the "leave-one-patient-out" approach excludes all the data of the patient to be evaluated from the training set, and therefore, solely relies on the other patients to make predictions. Results obtained in terms of average AUC show that after normalization, infarcted and non-infarcted tissue can, with a reasonable confidence, be predicted across patients.

The proposed study is not only useful to identify the optimal size of the regional model for a given perfusion map, but may also serve as a starting point to help us understand the limitations of current perfusion maps and to identify in which cases other factors may improve the predictions. While a correct prediction tells us that the relation between different PWI parameters and the outcome of the tissue can be captured by the model, a prediction error may originate from several technical errors (co-registration of images, normalization, classifier, data sampling, perfusion map) or come from physiological reasons (quality of collaterals, degree of success of arterial recanalization intervention). For example, in the case of an arterial occlusion, the infarct core might not grow after an unsuccessful intervention (failed opening of the vessel) due to good collateral blood supply to the territory. There is, therefore, a margin for improvement by taking into account additional physiological parameters (*e.g.* collateral flow) and a larger dataset.

## 5. Acknowledgments

This work was supported by the National Institutes of Health [K23-NS054084 and P50-NS044378 to D.S.L.] and [R01-NS066008 to X.H.].

## 6. References

Cai, D., He, X. & Han, J. (2007). Spectral Regression for Efficient Regularized Subspace Learning, *ICCV*.

Calamante, F., Christensen, S., Desmond, P. M., Ostergaard, L., Davis, S. M. & Connelly, A. (2010). The physiological significance of the time-to-maximum (Tmax) parameter in perfusion MRI, *Stroke* 41: 1169–1174.

Chemmanam, T., Campbell, B. C., Christensen, S., Nagakane, Y., Desmond, P. M., Bladin, C. F., Parsons, M. W., Levi, C. R., Barber, P. A., Donnan, G. A. & Davis, S. M. (2010). Ischemic diffusion lesion reversal is uncommon and rarely alters perfusion-diffusion mismatch, *Neurology* 75: 1040–1047.

Chen, F., Liu, Q., Wang, H., Suzuki, Y., Nagai, N., Yu, J., Marchal, G. & Ni, Y. (2008). Comparing two methods for assessment of perfusion-diffusion mismatch in a rodent model of ischaemic stroke: a pilot study, *Br J Radiol* 81: 192–198.

Fisher, M. & Ginsberg, M. (2004). Current concepts of the ischemic penumbra: introduction, *Stroke* 35: 2657–2658.

Hacke et al, W. (2008). Thrombolysis with alteplase 3 to 4.5 hours after acute ischemic stroke, *N. Engl. J. Med.* 359(13): 1317–1329.

Heiss, W. & Sobesky, J. (2005). Can the penumbra be detected: MR versus PET imaging, *J Cereb Blood Flow Metab* 25: S702.

Huang, S., Shen, Q. & Duong, T. Q. (2010). Artificial neural network prediction of ischemic tissue fate in acute stroke imaging, *J Cereb Blood Flow Metab* .

Jonsdottir, K., Ostergaard, L. & Mouridsen, K. (2009). Predicting Tissue Outcome From Acute Stroke Magnetic Resonance Imaging: Improving Model Performance by Optimal Sampling of Training Data, *Stroke* 40: 3006–3011.

Kidwell, C. S., Alger, J. R. & Saver, J. L. (2004). Evolving Paradigms in Neuroimaging of the Ischemic Penumbra, *Stroke* 35: 2662–2665.

Maree, R., Geurts, P., Piater, J. & Wehenkel, L. (2005). Random subwindows for robust image classification, *CVPR*, Vol. 1, pp. 34–40.

Nguyen, V., Pien, H., Menenzes, N., Lopez, C., Melinosky, C., Wu, O., Sorensen, A., Cooperman, G., Ay, H., Koroshetz, W., Liu, Y., Nuutinen, J., Aronen, H. & Karonen, J. (2008). Stroke Tissue Outcome Prediction Using A Spatially-Correlated Model, *PPIC*.

Olivot, J. M., Mlynash, M., Zaharchuk, G., Straka, M., Bammer, R., Schwartz, N., Lansberg, M. G., Moseley, M. E. & Albers, G. W. (2009). Perfusion MRI (Tmax and MTT) correlation with xenon CT cerebral blood flow in stroke patients, *Neurology* 72: 1140–1145.

Olivot, J., Mlynash, M., Thijs, V., Purushotham, A., Kemp, S., Lansberg, M., Wechsler, L., Gold, G., Bammer, R., Marks, M. & Albers, G. (2009). Geography, structure, and evolution of diffusion and perfusion lesions in Diffusion and perfusion imaging Evaluation For Understanding Stroke Evolution (DEFUSE), *Stroke* 40(10): 3245–3251.

Rose, S., Chalk, J., Griffin, M., Janke, A., Chen, F., McLachan, G., Peel, D., Zelaya, F., Markus, H., Jones, D., Simmons, A., O'Sullivan, M., Jarosz, J., Strugnell, W., Doddrell, D. & Semple, J. (2001). MRI based diffusion and perfusion predictive model to estimate stroke evolution, *Magnetic Resonance Imaging* 19(8): 1043–1053.

Scalzo, F., Hao, Q., Alger, J., Hu, X. & Liebeskind, D. (2010). Tissue Fate Prediction in Acute Ischemic Stroke Using Cuboid Models, *LNCS* 6454: 292–301.

Scalzo, F., Xu, P., Asgari, S., Bergsneider, M. & Hu, X. (2009). Regression analysis for peak designation in pulsatile pressure signals, *Med Biol Eng Comput* 47: 967–977.

Scalzo, F., Xu, P., Asgari, S., Kim, S., Bergsneider, M. & Hu, X. (2010). Robust Peak Recognition in Intracranial Pressure Signals, *Biomed Eng Online* 9: 61.

Schaefer, P., Barak, E., Kamalian, S., Romero, J., Koroshetz, W., Gonzalez, R. & Lev, M. (2007). Visual estimation of mri core/penumbra mismatch, versus quantitative measurement, unnecessarily excludes patients from thrombolytic clinical trials, *Stroke* 38: 453–607.

Schlaug, G., Benfield, A., Baird, A. E., Siewert, B., Lovblad, K. O., Parker, R. A., Edelman, R. R. & Warach, S. (1999). The ischemic penumbra: operationally defined by diffusion and perfusion MRI, *Neurology* 53: 1528–1537.

Shen, Q. & Duong, T. (2008). Quantitative Prediction of Ischemic Stroke Tissue Fate, *NMR Biomedicine* 21: 839–848.

Shen, Q., Ren, H., Fisher, M. & Duong, T. (2005). Statistical prediction of tissue fate in acute ischemic brain injury, *J Cereb Blood Flow Metab* 25: 1336–1345.

Siegel, S. & Castellan, N. (1988). *Nonparametric statistics for the behavioral sciences*, second edn, McGraw–Hill, Inc.

Smith., S. (2002). Fast robust automated brain extraction, *Human Brain Mapping* 17(3): 143–155.

Wu, O., Koroshetz, W., Ostergaard, L., Buonanno, F., Copen, W., Gonzalez, R., Rordorf, G., Rosen, B., Schwamm, L., Weisskoff, R. & Sorensen, A. (2001). Predicting tissue outcome in acute human cerebral ischemia using combined diffusion- and perfusion-weighted MR imaging, *Stroke* 32(4): 933–42.

Wu, O., Sumii, T., Asahi, M., Sasamata, M., Ostergaard, L., Rosen, B., Lo, E. & Dijkhuizen, R. (2007). Infarct prediction and treatment assessment with MRI-based algorithms in experimental stroke models, *Journal of Cerebral Blood Flow and Metabolism* 27: 196–204.

Yoo, A. J., Barak, E. R., Copen, W. A., Kamalian, S., Gharai, L. R., Pervez, M. A., Schwamm, L. H., Gonzalez, R. G. & Schaefer, P. W. (2010). Combining acute diffusion-weighted imaging and mean transmit time lesion volumes with NIHSSS improves the prediction of acute stroke outcome, *Stroke* 41: 1728–1735.

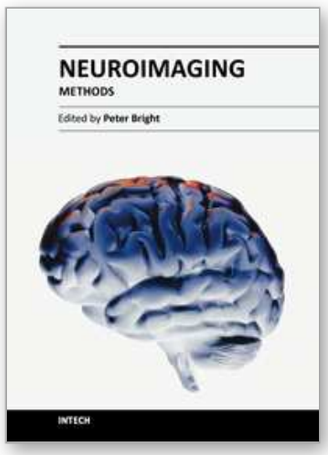


**Neuroimaging - Methods**

Edited by Prof. Peter Bright

ISBN 978-953-51-0097-3
Hard cover, 358 pages
**Publisher** InTech
**Published online** 17, February, 2012
**Published in print edition** February, 2012

Neuroimaging methodologies continue to develop at a remarkable rate, providing ever more sophisticated techniques for investigating brain structure and function. The scope of this book is not to provide a comprehensive overview of methods and applications but to provide a 'snapshot' of current approaches using well established and newly emerging techniques. Taken together, these chapters provide a broad sense of how the limits of what is achievable with neuroimaging methods are being stretched.

**How to reference**

In order to correctly reference this scholarly work, feel free to copy and paste the following:

Fabien Scalzo, Xiao Hu and David Liebeskind (2012). Tissue Fate Prediction from Regional Imaging Features in Acute Ischemic Stroke, Neuroimaging - Methods, Prof. Peter Bright (Ed.), ISBN: 978-953-51-0097-3, InTech, Available from: http://www.intechopen.com/books/neuroimaging-methods/tissue-fate-prediction-from-regional-imaging-features-in-acute-ischemic-stroke

INTECH
open science | open minds

**InTech Europe**
University Campus STeP Ri
Slavka Krautzeka 83/A
51000 Rijeka, Croatia
Phone: +385 (51) 770 447
Fax: +385 (51) 686 166
www.intechopen.com

**InTech China**
Unit 405, Office Block, Hotel Equatorial Shanghai
No.65, Yan An Road (West), Shanghai, 200040, China
中国上海市延安西路65号上海国际贵都大饭店办公楼405单元
Phone: +86-21-62489820
Fax: +86-21-62489821

IntechOpen